



**Planar Imaging of Density Interfaces  
Accelerated by Strong Shocks**

**M.H. Anderson, B.P. Puranik,  
J.G. Oakley, R.R. Peterson, R. Bonazza**

**July 1999**

**UWFDM-1115**

Prepared for the 22nd International Symposium on Shock Waves, Imperial College, London, UK, July 18-23, 1999.

***FUSION TECHNOLOGY INSTITUTE***

***UNIVERSITY OF WISCONSIN***

***MADISON WISCONSIN***

### **DISCLAIMER**

This report was prepared as an account of work sponsored by an agency of the United States Government. Neither the United States Government, nor any agency thereof, nor any of their employees, makes any warranty, express or implied, or assumes any legal liability or responsibility for the accuracy, completeness, or usefulness of any information, apparatus, product, or process disclosed, or represents that its use would not infringe privately owned rights. Reference herein to any specific commercial product, process, or service by trade name, trademark, manufacturer, or otherwise, does not necessarily constitute or imply its endorsement, recommendation, or favoring by the United States Government or any agency thereof. The views and opinions of authors expressed herein do not necessarily state or reflect those of the United States Government or any agency thereof.

# Planar Imaging of Density Interfaces Accelerated by Strong Shocks

M.H. Anderson, B.P. Puranik, J.G. Oakley, R.R. Peterson, R. Bonazza

Department of Engineering Physics, University of Wisconsin-Madison, Madison, WI 53706, USA

**Abstract:** Shock tube experiments have been performed in the past at many different institutions and in a great variety of configurations to study the evolution of the perturbations on a shock-accelerated interface (Richtmyer-Meshkov instability). Two limitations common to all previous experimental investigations were posed by the size and structural capability of the shock tubes being used. Here we present the first experiments performed in a new vertical square shock tube facility designed specifically to overcome these limitations. Both continuous (diffuse) and discontinuous (sharp) interfaces are studied. Incident shock Mach numbers are in the 2-4 range, with the driven and test gases initially at atmospheric pressure. Shadowgraphy and planar (Mie scattering and Rayleigh scattering) imaging of the interface are presented.

**Key words:** Shock-interface interactions, Richtmyer-Meshkov instability, Rayleigh scattering

## 1. Introduction and Motivation

In inertial confinement fusion experiments, the instability of any perturbations on a density interface impulsively accelerated by a shock wave (Richtmyer-Meshkov instability) (Richtmyer (1961), Meshkov (1970)) is one of the important obstacles that must be overcome to achieve useful energy yield in the laser-driven implosion of microtargets filled with deuterium-tritium (DT) ice. The R-M instability is a fundamental fluid instability which also appears in other phenomena such as supersonic combustion and supernova explosions.

The Richtmyer-Meshkov (R-M) instability has been studied extensively over the last 30 years. Most of the experimental investigations of the R-M instability were carried out in shock tubes (e.g. Jacobs et al. (1995)). Two limitations common to all previous shock tube investigations of the R-M instability were posed by the size and structural capability of the shock tubes being used. The structural capability of most facilities usually limited the maximum strength of the shock being released into gases at atmospheric pressure to  $M \leq 2.0$ . In order to accelerate the density interface with stronger shocks, the

initial pressure of the driven and test gases could be lowered so that, even at high incident Mach numbers, the maximum load capability of the tube would not be exceeded. This, however, causes the interaction of the shock reflected off the tube's end wall with the boundary layers formed by the passage of the incident wave to produce large wall vortices (Fig. 1). These vortices exert a strain on the interface and thus introduce uncertainties in the instability growth measurements. The effect of the vortices on the interface behavior increased as the initial density decreased and was proportionally more important in shock tubes of small cross-section (Bonazza and Sturtevant(1996)).

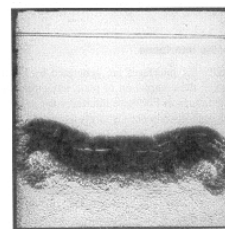


**Figure 1.** Schlieren Image of a Wall Vortex at a Shocked Interface

The linear stage of the R-M instability is characterized by the amplitude of the perturbations being much smaller than the wavelength ( $\eta \ll \lambda$ ). When the amplitude of the perturbations is no longer small compared to the wavelength, a nonlinear stage develops. It is characterized by a decrease in the growth rate, onset of secondary Kelvin-Helmholtz instability, interaction between different modes (if a multimode initial perturbation is present) and a distortion of the initially sinusoidal interface into what is termed as “spikes” and “bubbles” (Hecht et al. (1994)). Although the previous experimental work characterizes the linear stage well, there is still need for experimental data to understand the nonlinear stage of growth. Such a database can be used to benchmark analytical models and numerical simulations (e.g. Zhang and Sohn (1997)). Also, experimental data are needed for strong incident shocks to quantify the effects of compressibility on the R-M instability.

## 2. Experimental Facility

### 2.1. The Wisconsin Shock Tube

A new shock tube has been fabricated for the study of the R-M instability. The tube is vertical, with a large square inner cross-section ( $25\text{ cm} \times 25\text{ cm}$ ) and is 9.2 m long. The square cross-section provides the parallel walls necessary for flow visualization without resorting to a structurally weak tube extension (Meshkov (1970)). It has a structural capability to withstand a 20 MPa pressure load. Thus, strong shocks can be fired into a driven section initially at atmospheric pressure. High initial pressure in the driven section is useful in reducing the secondary effects of the wall vortices, since the value of the kinematic viscosity of the driven gas is higher at atmospheric pressure than that at subatmospheric pressures. The vertical orientation of the tube allows preparation of a continuous interface between gases of different densities making use of gravitational stratification. Figure 2 shows the tube assembly.

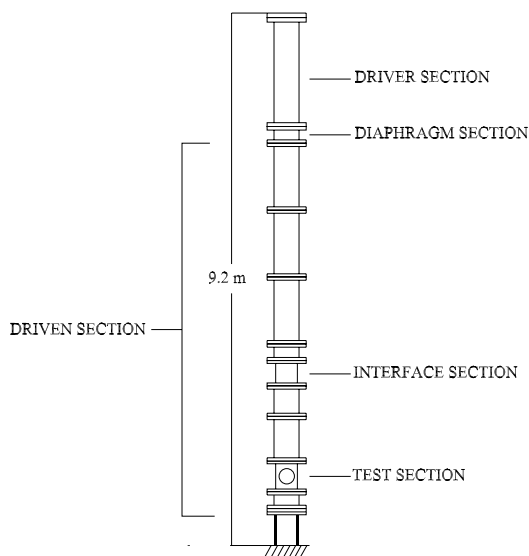


**Figure 2.** Schematic of the Wisconsin Shock Tube

The driver section is made from a circular, chrome-plated carbon steel pipe, 42 cm ID, 1.9 cm thick and 2 m long. It is equipped with four ignition tubes mounted inside the driver section, capable of igniting a stoichiometric mixture of oxygen and hydrogen diluted in helium, to produce high pressure and temperature driver conditions.

Figure 3 shows the cross-section of the driven section. An internal liner, consisting of four stainless steel plates 1 cm thick, welded together, is supported by a concrete matrix contained in a circular carbon steel pipe, 42 cm ID to form a segment of the driven sec-

tion. These segments are then capped with a class 300# A-105 flange welded to the top and bottom of the tube. This allows any two of the nine sections to be bolted together.

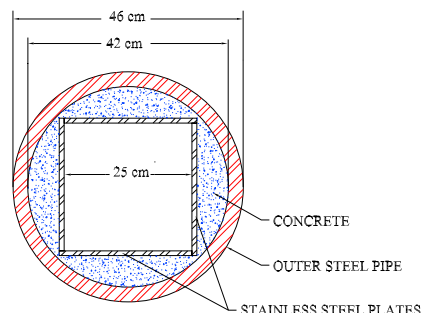


**Figure 3.** Schematic of the Cross-Section of the Driven Section

The test section consists of four steel plates, chrome plated on their inside surface, 7 cm thick, welded together to form a box with a 25 cm square inside cross-section. The test section contains two circular ports 28 cm in diameter, on opposite sides. Fused quartz windows, 24 cm in diameter and 9 cm thick, are mounted in these ports for optical access.

The tube also contains an “interface section”, specifically designed for the study of shock-interface interactions. It consists of four steel plates, chrome plated on their inside surface, approximately 7 cm thick, welded together to form a box with a 25 cm square inside cross-section. An interface between two gases of different densities is formed in this section. A pneumatic system is used to retract a thin stainless steel plate (0.381 mm thickness) producing the continuous (diffuse) interface, while a frame holding a mylar or nitrocellulose membrane can be inserted in the interface section to produce the discontinuous (sharp) interface.

The modular structure of the shock tube allows the placement of the interface section, the test section and the end wall at various mutual distances, thus allowing for the visualization of the interface after the initial shock acceleration at various delay times. The end wall of the shock tube contains a circular, fused quartz window. A laser sheet can be projected upward for planar imaging of the interface through this window. The whole shock tube assembly is supported on three cylindrical, solid steel legs, 18 cm diameter, 30 cm long. The legs, in turn, are anchored in a  $8\text{ m}^3$  concrete foundation.

### 2.2. Diagnostics

In the first series of flow visualization experiments, either a modified Continuum (Surelite II-PIV) pulsed

Nd:YAG laser or an arc discharge lamp is used as a light source for the imaging. The laser consists of two laser cavities capable of delivering 200 mJ/pulse (and hence 400 mJ/pulse when the beams are super-imposed) at  $\lambda=532$  nm. The pulse width is 10 ns. The laser has been modified from its original repetition mode to a “single shot” mode. This allows the laser to stay charged for a long time. It can then be pulsed on an external triggering signal. The Xenon Inc. Model-437B short duration 20 ns broad spectrum, arc discharge lamp was used in some experiments to attain a more spatially uniform light source than could be achieved with the laser. A 16-bit CCD camera (Spectra Video Series, by Pixel Vision) is used to capture the images. It has a back-lit,  $1024 \times 1024$  pixel array, a thermo-electrically cooled sensor and a low speed (40 kHz) transfer rate that guarantee low dark current and readout noise ( $1 e^-/\text{pix s}$  and  $5\text{-}8 e^-$  rms respectively, @  $-45^\circ \text{C}$ ). A narrow band ( $\pm 5$  nm) green filter is used with the camera to reject all extraneous light when planar Rayleigh scattering measurements are performed. An HP-Infinium 4 channel digital oscilloscope with a sampling rate 1 GHz per channel is used to record the pressure traces from the piezoelectric pressure transducers, flush mounted on the inner wall of the shock tube. The pressure transducer signal is used to trigger the laser to pulse, after an appropriate delay, to capture the image of the shock-accelerated interface. One image is obtained per event.

### 2.2.1. Shadowgraphy

The Xenon Inc. arc lamp is used for shadowgraphy, since it provides a more spatially uniform light beam than that provided by the laser. The light beam from the arc lamp is expanded by a plano-concave lens (focal length -15 mm), collimated by a plano convex lens (focal length 500 mm) to a diameter of 212 mm, passed through the test section and projected on a screen. The camera is focused on the screen to capture the image.

### 2.2.2. Planar Mie Scattering

Planar imaging of the flowfield is advantageous since it provides more quantitative data than shadowgraphy. In planar imaging, the flow is interrogated by a thin sheet of laser light providing a highly localized data, unlike shadowgraphy which provides line-of-sight integrated information. Planar Mie scattering is employed to visualize the instability growth. A laser sheet is projected vertically upward through the window in the end wall of the tube, using cylindrical optics. The

sheet is focused approximately in the center of the test section. The thickness of the sheet is approximately 0.3 mm and the width is about 10 cm. Just before firing the shock, one of the gases forming the interface is injected with a small amount of cigarette smoke and the Mie scattering signal off the smoke particles is collected at right angles to the plane of the laser sheet. The amount of smoke is negligibly small compared to the amount of the gas. Hence the density of the gas is not affected. Mie scattering measurements can be used to study the growth rates of the instability. Since the flow tracking fidelity of the smoke particles in such high speed flows is questionable, quantitative densitometry measurements cannot be performed with Mie scattering. However, the Mie scattering images provide qualitative information on the mixing due to the instability.

### 2.2.3. Planar Rayleigh Scattering

Rayleigh scattering is a powerful technique that can be employed to study mixing between gases, such as in the case of R-M instability. In particular, consider two gases  $A$  and  $B$ . The Rayleigh signal obtained by scattering off this mixture is given by,

$$P_{Ray} \sim n \left[ \chi_A \left( \frac{\partial \sigma}{\partial \Omega} \right)_A + \chi_B \left( \frac{\partial \sigma}{\partial \Omega} \right)_B \right] \quad (1)$$

where  $\chi_A$  and  $\chi_B$  are the mole fractions of  $A$  and  $B$  respectively,  $\left( \frac{\partial \sigma}{\partial \Omega} \right)$  is the differential cross-section of the gas for Rayleigh scattering and  $n$  is the total number density. Also, note that,

$$\chi_A = 1 - \chi_B . \quad (2)$$

Therefore, once the Rayleigh power is estimated, the mole fractions of the mixing gases can be determined using Eqs. 1 and 2. The scattering gas can be subjected to different pressures and a calibration on the Rayleigh signal can be obtained. This calibration can be used to map the pixels in the flowfield image into individual density values. Such a densitometry technique would then provide quantitative data on the shock-induced mixing.

A laser sheet is projected vertically upward from the window in the end wall of the tube, as in the case of Mie scattering. The Rayleigh scattering signal is collected at right angles to the plane of the sheet. Since the strength of the Rayleigh signal is orders of magnitude smaller than that for Mie scattering, the width of the laser sheet is reduced to 8 cm to increase the energy density of the incident light. Furthermore, the Rayleigh signal suffers from the presence of any impurity particles such as membrane fragments. Hence, only continuous interfaces prepared using the retractable plate are studied with Rayleigh scattering.

### 3. Experimental Results

#### 3.1. Shadowgraphy

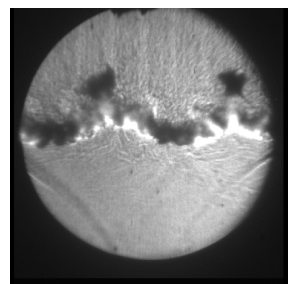
Shadowgraphy is used as a preliminary diagnostic for imaging the shocked interfaces. A discontinuous interface is prepared using the mylar membrane, supported in an aluminum frame which is placed in the interface section. The membrane is shaped into a sinusoid form by machining the supporting surfaces of the two halves of the frame into a sinusoidal shape. Thin nylon wires (0.23 mm thickness) are placed at regular intervals (1.27 cm) along the sinusoidal portion of the frame, across the width, to support and maintain the membrane in shape. The wires also help in rupturing the membrane into small pieces. The wavelength of the machined sine wave is 6.35 cm while the amplitude is 0.635 cm. The field of view in all shadowgraphy images is such that a central area of the test section covering two wavelengths of the sinusoidal perturbation is visible. Due to the limited number of support wires, the actual membrane profile in the center of the shock tube is a triangular wave instead of a sinusoidal wave, with a reduced amplitude due to stretching of the membrane. Figure 4 shows the actual profile of the membrane. This profile serves as the initial condition for the instability.



**Figure 4.** Actual Membrane Profile in the Plane of the Laser Sheet

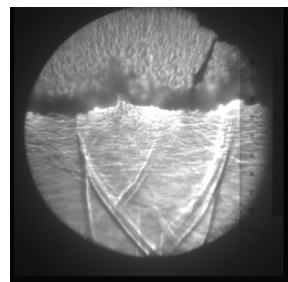
Figure 5 shows a shocked air-CO<sub>2</sub> discontinuous interface (pre-shock Atwood number of 0.206) 1.134 ms after the initial shock acceleration. The Mach number of the incident shock wave is 2.02 in air. The diameter of the field of view is 13.97 cm and contains about two wavelengths of the initial perturbation. It can be seen from the image that the perturbation amplitude has grown while the wavelength has remained approximately constant. The incipience of the nonlinear stages of growth is evident by the formation of “spikes” of CO<sub>2</sub> (heavy fluid) interleaved by “bubbles” of air (light fluid). Furthermore, the interface has thickened due to the mixing induced by the instability. The mylar membrane fragments travel with the interface and are present at the trough and peak of the sinusoid. The membrane pieces may affect the growth of the instability by introducing secondary motions. Further experiments at higher Mach numbers are planned to investigate if the membrane gets pyrolyzed due to shock heating.

Figure 6 shows a shocked N<sub>2</sub>-CO<sub>2</sub> discontinuous in-



**Figure 5.** Shocked air-CO<sub>2</sub> Discontinuous Interface 1.134 ms after Interaction with a Mach 2.02 Shock Wave

terface (pre-shock Atwood number of 0.222) 0.667 ms after the initial shock acceleration. The Mach number of the incident shock wave is 2.90 in nitrogen. It can be seen that the perturbation has evolved into the spike and bubble form, though the growth appears smaller than in the previous image. This is partly due to the fact that the delay time between initial shock acceleration and capturing of the image is less than that in the previous case. Also, stronger compressibility effects at higher Mach number may play a role in the apparently lower growth rate. The lines below the interface are thought to be higher order reflections of the shock off the membrane, support wires and the side walls of the tube. The strong incident shock in this experiment produces density gradients associated with the higher order reflections that are strong enough to appear in the shadowgraphy image. The membrane pieces are still present at the interface location; however, they are difficult to see in this image.



**Figure 6.** Shocked N<sub>2</sub>-CO<sub>2</sub> Discontinuous Interface 0.667 ms after Interaction with a Mach 2.90 Shock Wave

Figure 7 shows a shocked He-CO<sub>2</sub> discontinuous interface (pre-shock Atwood number of 0.833) 0.859 ms after the initial shock acceleration. The Mach number of the incident shock wave is 1.90 in helium. Due to the high Atwood number, the instability rapidly reaches the nonlinear stage. It can be seen that large spikes of CO<sub>2</sub> are protruding in helium. Also, it can be noted that the helium bubbles are much flatter compared to the bubbles in earlier cases.

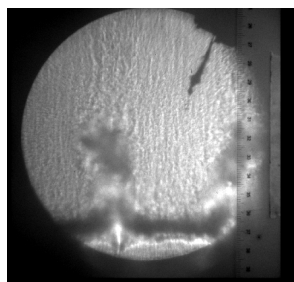


**Figure 7.** Shocked He-CO<sub>2</sub> Discontinuous Interface 0.859 ms after Interaction with a Mach 1.90 Shock Wave

### 3.2. Planar Mie Scattering

Figure 8 shows a Mie scattering image of a shocked He-CO<sub>2</sub> discontinuous interface (pre-shock Atwood number of 0.833) 0.737 ms after the initial shock acceleration. The Mach number of the incident shock wave is 2.08 in helium. Just prior to the firing of the shock, a small amount of smoke is injected in CO<sub>2</sub> below the membrane. The laser sheet thickness is 0.3 mm and its width is 10 cm. The spike and bubble structure is clearly evident in this localized imaging. A thin region, showing small scale mixing, can also be identified at the interface location and the thickening of the interface is evident. The Mach number for this case is comparable to that in Fig. 7. It can be seen that the two images are similar. The membrane pieces can be identified as the bright areas near the peaks and the troughs. The membrane pieces seem to follow the motion of the gases and conform to the bubble and spike shapes.

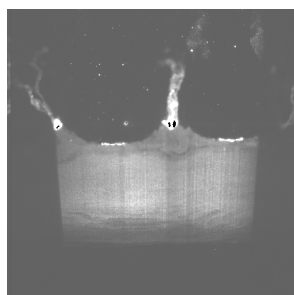


**Figure 8.** Shocked He-CO<sub>2</sub> Discontinuous Interface 0.737 ms after Interaction with a Mach 2.08 Shock Wave

### 3.3. Planar Rayleigh Scattering

Figure 9 shows a Rayleigh scattering image of a shocked He-CO<sub>2</sub> continuous interface (pre-shock Atwood number of 0.833) 0.737 ms after the initial shock acceleration. The Mach number of the incident shock wave is 2.08 in helium. The interface is created by retracting a thin (0.381 mm thickness) metal plate initially separating helium (at the top) and CO<sub>2</sub> (at the bottom), both at atmospheric pressure. The delay time between the completion of the plate retraction

and firing of the shock is 1 second. The retraction of the plate creates a fairly flat interface. At present, experiments are being carried out to characterize the initial conditions produced by the plate retraction, after various delay times, using Mie and Rayleigh scattering. This information is important to serve as the initial conditions for computer simulations, to test the repeatability of the creation of the initial conditions, and to obtain quantitative data on the mixing and instability growth rates from the images.

The width of the laser sheet is about 8 cm and its thickness is about 0.3 mm, in the center of the test section. The interface between the helium and CO<sub>2</sub> is clearly evident due to the differential scattering by the two gases (CO<sub>2</sub> scatters light 140 times more than helium).

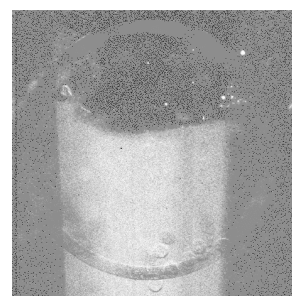


**Figure 9.** Shocked He-CO<sub>2</sub> Continuous Interface 0.737 ms after Interaction with a Mach 2.08 Shock Wave

## 4. Numerical Simulation

A numerical simulation of the test in Fig. 8 (Mach 2.08, helium/CO<sub>2</sub>) is conducted with an AMR (adaptive mesh refinement) code, RAGE (Radiation Adaptive Grid Eulerian). A description of the code can be found in Baltrusaitis et al. (1996), Holmes et al. (1999). The initial conditions imposed in the simulation are similar to those discussed in Fig. 4, with the exception of the membrane and the wires supporting it. Figure 10 shows the results of the simulation at four time steps, showing the density contours. Figure 10A is slightly before the shock wave contacts the interface and the subsequent figures are at times approximately 0.3, 0.7 and 1 ms after shock interface interaction. Figure 10B shows the initial growth of “spikes” of the CO<sub>2</sub> into the lighter helium gas above. The height of the spike is approximately 5 cm and there is a slight indication of the beginning of vortices formed from Kelvin-Helmholtz instabilities on the top of the spikes. Figure 10C is at approximately the same delay time as the Mie scattering photograph of Fig. 8. The simulation predicts mushroom shaped structures indicative of the Kelvin-Helmholtz instabilities. The height of the spikes have also grown to approximately 10 cm and there appears

to be some interaction between adjacent spikes. Figure 10D indicates significant interaction and mixing between adjacent spikes and the rest of the gas. Qualitatively the simulation is quite similar to the experimental data shown in Fig. 8 (0.737 ms after shock acceleration). By visual comparison, the data looks most similar to Fig. 10B of the simulation (0.3 ms) rather than that of Fig. 10C (same time after interaction) since there are no mushroom shaped structures in the experimental image and the size of the spikes are approximately the same as those of Fig. 10B (5 cm). Although only one experimental time is shown, this could indicate that the simulation is evolving at a more rapid rate than that of the actual experiment or that slight differences in the initial conditions alter the growth rate. It could also be that the presence of the membrane is slowing the growth of the perturbation. Further studies are in progress to look at the experimental growth rate of this instability.

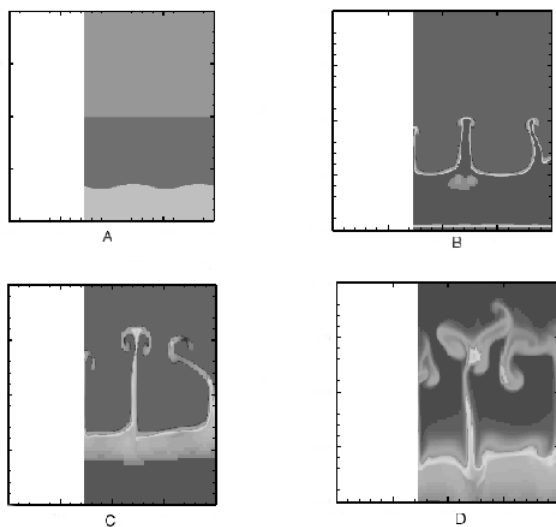


**Figure 10.** Numerical simulation of the Richtmyer-Meshkov Instability with the RAGE (Radiation Adaptive Grid Eulerian) code. Plot A is prior to shock acceleration and plots B, C and D are at 0.3, 0.7 and 1.0 ms after shock acceleration respectively.

## 5. Conclusion

A new, vertical square shock tube has been fabricated to study the Richtmyer-Meshkov instability. In the first series of experiments, shadowgraphy is used as a preliminary diagnostic to visualize shocked interfaces. Preliminary experiments with planar imaging such as Mie scattering and Rayleigh scattering images are performed and the data is compared to the shadowgraphy data along with numerical simulations. Further experiments are in progress to study the time evolution of relevant geometrical parameters such as the amplitude

of the interfacial perturbations and thickening of the interface due to the shock-induced mixing, in the non-linear stages of growth. Mie and Rayleigh scattering measurements will be performed on the images and quantitative densitometry techniques will be used to extract the growth rates for the amplitude and the thickness. The experimental results will be further compared to the results from numerical simulations performed with the AMR codes such as RAGE.

**Acknowledgement.** The authors would like to thank R. P. Weaver and M. L. Gittings of LANL for their help with RAGE calculations and ASCI computer time.

This work was supported by DOE Grant No. DE-FG03-98DP00207.

## References

- Baltrusaitis RM, Gittings ML, Weaver RP, Benjamin RF, Budzinski JM (1996) Simulation of shock generated instabilities. *Physics of Fluids*, 8(9):2471-2483
- Bonazza R, Sturtevant B (1996) X-Ray measurements of growth rates at a gas interface accelerated by shock waves. *Physics of Fluids*, 8(9):2496-2512
- Hecht J, Alon U, Shvarts D (1994) Potential flow models of Rayleigh-Taylor and Richtmyer-Meshkov bubble fronts. *Physics of Fluids*, 6(12):4019-4030
- Holmes RL, Zoldi CA, Weaver RP, Gittings ML, Clover MR (1999) Simulations of Richtmyer-Meshkov instability in two and three dimensions. ISSW22 paper No. 4480
- Jacobs JW, Klein DL, Jenkins DG and Benjamin RF (1995) Nonlinear growth of the shock-accelerated instability of a thin fluid layer. *Journal of Fluid Mechanics*, 295:23-42
- Meshkov EE (1970) Instability of a shock wave accelerated interface between two gases. NASA technical translation, NASA TT F-13, 074.
- Richtmyer RD (1961) Taylor instability in shock accelerated compressible fluids. *Comm. on Pure and App. Math.*, 13:297-319
- Zhang Q, Sohn S (1997) Nonlinear theory of unstable fluid mixing driven by shock wave. *Physics of Fluids* 9(4):1106-1124